Protein-protein Binding Detection with Nanoparticle Photonic Crystal Enhanced Microscopy (NP-PCEM)*

Yue Zhuo, *Student Member, IEEE,* Limei Tian, Weili Chen, Hojeong Yu, Srikanth Singamaneni,
Brian T. Cunningham, *Fellow, IEEE*

Abstract—We demonstrate a novel microscopy-based biosensing approach that utilizes a photonic crystal (PC) surface to detect protein-protein binding with the functionalized nanoparticles as tags. This imaging approach utilizes the measurement of localized shifts in the resonant wavelength and resonant reflection magnitude from the PC biosensor in the presence of individual nanoparticles. Moreover, it substantially increases the sensitivity of the imaging approach through tunable localized surface plasmon resonant frequency of the nanoparticle matching with the resonance of the PC biosensor. Experimental demonstrations of photonic crystal enhanced microscopy (PCEM) imaging with single nanoparticle resolution are supported by Finite-Difference Time-Domain (FDTD) computer simulations. The ability to detect the surface adsorption of individual nanoparticles as tags offers a route to single molecule biosensing with photonic crystal biosensor in the future.

I. INTRODUCTION

Identification of protein-protein binding is essential to the development and evaluation of new pharmaceuticals, and also critical to the biological genetic approaches for elucidating complex signal pathways. Nanoparticles (NP) have great potential as biosensing tags for protein-protein binding detection due to their nanometer scale size (comparable to biological molecules or antibodies), especially for gold nanoparticle (AuNP) with the amenability of synthesis and functionalization, less toxicity and absence of photobleaching. While many biosensing approaches are capable of sensing the adsorption of large numbers of nanoparticles, several approaches are capable of detecting the presence of a single nanoparticle, if the particle is adsorbed to a specific active location [1-3]. However, it is often difficult to direct the analytes to precise locations on a substrate surface where a biosensor has sensitivity. One approach to overcoming this limitation is to utilize a biosensor surface in which the entire surface area is active as a sensor. Through the use of an imaging detection approach, the adsorption of analyte upon any region within the field of view may be measured. Imaging-based biodetection utilizing optical sensors has been demonstrated using surface plasmon resonance [4-7], photonic crystal biosensors [8-12], and dielectric thin film interference sensors [13-16]. Such
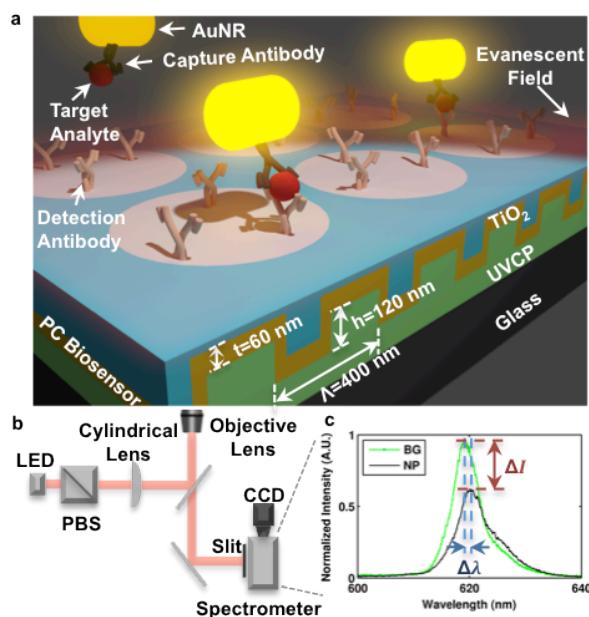
Figure 1. Principle of Nanoparticle Photonic Crystal Enhanced Microscopy (NP-PCEM). (a) Schematic diagram of protein-protein binding detection with nanorods as tags on a photonic crystal (PC) surface. (b) Instrument schematic of the PCEM. (c) Example spectra with a peak wavelength value (PWV) shift and a peak intensity value (PIV) change with/without a detected nanoparticle on PC surface (BG-background, NP-nanoparticle).

approaches are advantageous because analytes that produce highly localized changes in dielectric permittivity (such as cells, virus particles, or nanoparticles) may be detected, with the potential to observe the attachment of individual targets.

In this work, we apply a recently developed form of microscopy, termed "Nanoparticle Photonic Crystal Enhanced Microscopy" (NP-PCEM) to image the attachment of dielectric and metallic nanoparticles upon a photonic crystal (PC) surface [17]. We demonstrate that nanoparticles produce highly localized effects upon the PC resonant reflection spectrum that enable individually attached nanoparticles to be easily observed as small as $\sim 30 \times 30 \times 65$ nm^3. Furthermore, by matching the localized surface plasmon resonance (LSPR) of the gold nanorods (AuNR) to the PC resonance substantially increases sensitivity of this biosensing approach. Our ultimate goal is to apply individual nanoparticles as functionalized tags in "sandwich" style assays, which can be used to visualize the presence of individual captured analyte biomolecules upon a PC biosensor surface (Fig. 1a). NP-PCEM imaging offers an attractive alternative to detection using fluorescent nanoparticles, as NP-PCEM requires only low power broadband illumination, does not suffer from

photobleaching, can provide long-term time-course data, and can be utilized for any type of nanoparticle tags.

II. PRINCIPLE

A. Photonic Crystal Biosensor

A photonic crystal biosensor is a sub-wavelength grating structure consisting of a periodic arrangement of a low refractive index material coated with a high refractive index layer (Fig. 1a). When the PC is illuminated with a broadband light source, high order diffraction modes couple light into and out of the high index layer, destructively interfering with the zeroth-order transmitted light. At a particular resonant wavelength and incident angle, complete interference occurs and no light is transmitted, resulting in nearly 100% reflection efficiency. The resonant wavelength is modulated by the addition of biomaterial upon the PC surface, resulting in a shift to a higher wavelength. The electromagnetic standing wave that is generated at the PC surface during resonant light coupling inhibits lateral propagation, thus enabling neighboring regions on the PC surface to display a distinct resonant wavelength that is determined only by the density of biomaterial attached at that precise location. By measuring the resonant peak wavelength value (PWV) or peak intensity value (PIV) (Fig. 1c) on a pixel-by-pixel basis over a PC surface, a spatial PWV or PIV image of nanoparticle attachment may be recorded.

B. Tunable LSPR of AuNR

The optical extinction spectrum of a prolate spheroid (*e.g.,* nanorod) exhibits two district localized surface plasmon resonances, corresponding to the two unique modes of electron oscillation along transverse and longitudinal directions. The absorption cross-section of the prolate spheroid is derived from Mie theory by Richard Gans:

$$\sigma_{abs} = \frac{\omega}{3c}\varepsilon_m^{3/2}V\sum_j \frac{\left(1/P_j^2\right)\varepsilon_2}{\left\{\varepsilon_1+\left[(1-P_j)/P_j\right]\varepsilon_m\right\}^2+\varepsilon_2^2}. \tag{1}$$

Where, the sum over j involves the three dimensions of the nanorod. P_j (that includes P_A, P_B, and P_C) represents depolarization factors, where A>B=C for a nanorod. The depolarization values (P_j) depends on the aspect ratio of the nanorods as follows:

$$P_A = \frac{1-e^2}{e^2}\left[\frac{1}{2e}\ln\left(\frac{1+e}{1-e}\right)-1\right], \qquad P_B = P_C = \frac{1-P_A}{2}. \tag{2}$$

Where e is related to aspect ratio (R) as follows:

$$e = \left(1-\frac{1}{R^2}\right)^{1/2}. \tag{3}$$

As evident from (2), the depolarization factor along the longitudinal direction (P_A) exhibits a strong dependence on aspect ratio and decreases sharply with increasing aspect ratio. The reduction in the restoring force for the longitudinal plasmon mode with increase in the aspect of ratio of AuNR results in lowering its resonance frequency (or increasing LSPR wavelength). Thus, the longitudinal plasmon band of AuNR is highly sensitive to the aspect ratio of AuNR. In aqueous solution, the longitudinal plasmon resonance wavelength (λ_{max}) is linearly proportional to the aspect ratio (R) given by the following relationship:

$$\lambda_{max} = 95R + 420. \tag{4}$$

III. METHODS

A. Electromagnetic Modeling

The modeling of the electromagnetic field distribution around plasmonic nanorods is performed using 3D finite-difference time-domain (FDTD) technique with commercially available software (EM Explorer). FDTD simulations exploit the time and position dependence of Maxwell's equations to model electromagnetic waves in rectangular 3D cells of finite volume called Yee cells. To obtain the electromagnetic field distribution, a single AuNR of ~30×30×60 nm³ size is modeled in a simulation domain of 300×300×200 nm³ using p-polarized incident plane wave for illumination with Yee cell size of 2 nm. Perfectly matched layer (PML) absorbing boundary conditions are applied in all directions. The complex refractive index of gold at the extinction maximum wavelength is set to n_{Au}=0.18+i4.96.

Another commercially available simulation package (FDTD, Lumerical Solutions, Inc.) is employed to model the distribution of excited electromagnetic field on the PC surface. Similarly, a p-polarized uniform plane wave illuminates the structure at normal incidence with a magnitude of E=1 V/m. Two periods of the PC device are simulated, with periodic boundary conditions applied to the x extents (perpendicular to the grating lines) and PML boundary conditions in other directions (y, z). In this study, we choose a 1D UV-curable polymer structure (n_{poly}=1.5) with a sufficiently high grating depth (d=120 nm) to confine the near field emission intensity. The grating period (Λ=400 nm) and duty cycle (f=50%) of the PC biosensor are selected to support high Q-factor resonant modes at the specific wavelength (λ_{PC}=620 nm). The thickness (t=60 nm) of the deposited TiO₂ (n_{TiO2}=2.4) layer can be used to fine-tune the spectral location of the resonant modes.

B. PC Biosensor Fabrication

The PC biosensor is fabricated by a nanoreplica molding approach (Fig. 2). First, deep-UV lithography and reactive ion etching are used to produce a silicon wafer molding template with a negative image of the desired grating profile. Then, a thin layer of liquid epoxy polymer (UV-curable) is deposited between the wafer template and glass substrate
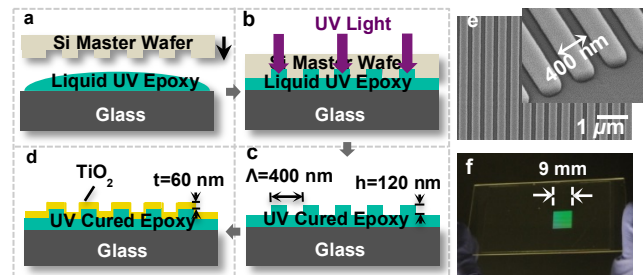
Figure 2. PC Fabrication Process. (a) First deposit a thin layer of liquid UV epoxy polymer between a Si wafer template and a glass substrate. (b) The epoxy is converted to a solid with UV light exposure. (c) The template is peeled away and the grating pattern is transferred to the glass. (d) A thin layer of sputter-deposited TiO2 film is applied over the grating structure. (e) SEM image of the PC surface. Inset: Zoomed in tiled SEM image. (f) Photo of a PC fabricated on a glass cover slip.
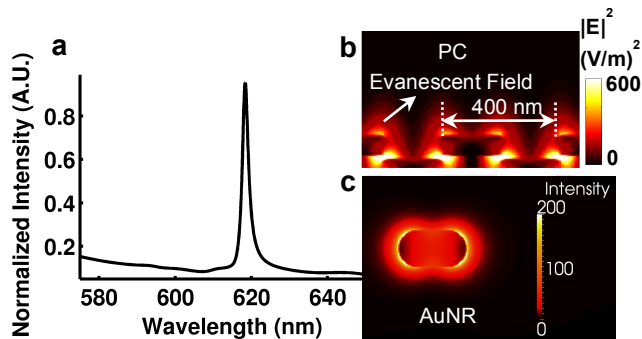
Figure 3. Computer simulations. FDTD simulations show (a) the reflection and (b) near field distributions of the PC biosensor surface. (c) E-field distribution around an AuNR.

and cured to solid status by exposing it to a high intensity UV lamp. Therefore, the nano-patterned surface is transferred to the glass substrate through epoxy polymer after peeling off the wafer template. Finally, a thin TiO_2 film is sputtered over the grating structure using a reactive RF sputtering machine (PVD 75, Kurt Lesker). Additionally, a thin SiO_2 layer (~20 nm in thickness) is deposited on the top of the PC device to protect the biosensor surface.

C. PCEM Imaging System

A simplified schematic diagram of PCEM imaging system is shown in Fig. 1b. To avoid light scattering and adsorption from the sample, PCEM imaging is performed via reflection from beneath the PC surface. The light source is a broadband LED (Thorlabs M617F1, $600 < \lambda < 650$ nm) coupled with optical fiber. The fiber output is collimated and filtered by a polarizing beamsplitter (PBS) and focused by a cylindrical lens. The microscope (Carl Zeiss Axio Observer Z1) is equipped with a 10× or 40× objective lens (Zeiss) plus an extra magnification lens (1.6×). Following the extra lens, a narrow slit aperture ($\lambda = 620$ nm, $\Delta\lambda = 30$ nm) is incorporated with a grating-based spectrometer (Acton Research), which is connected to a CCD camera (Photometrics Cascade, 512×512 pixels). The motorized stage (Applied Scientific Instruments, MS2000) enables scanning the sample with a selected increment per step. In this study, the effective pixel size is 0.6^2 μm^2 for a 10× objective lens.

D. Gold Nanorods Synthesis

AuNR is synthesized using a seed-mediated approach. Seed solution is prepared by adding 0.6 mL of an ice-cold sodium borohydride solution (10 mM) into 10 mL of 0.1 M cetyltrimethylammonium bromide (CTAB) and 2.5×10^{-4} M chloroauric acid ($HAuCl_4$) solution under magnetic stirring at room temperature. The color of the seed solution changes from yellow to brown. Growth solution is prepared by mixing 95 mL of CTAB (0.1 M), 0.5 mL of silver nitrate (10 mM), 5 mL of $HAuCl_4$ (10 mM), and 0.55 mL of ascorbic acid (0.1 M) in the same order. The solution is homogenized by gentle stirring. To the resulting colorless solution, 0.12 mL of freshly prepared seed solution is added and aged for two weeks at room temperature. Prior to use, the AuNR solution is centrifuged at 10, 000 rpm for 10 mins to remove excess CTAB and redispersed in nanopure water (18.2 MΩ-cm). The centrifugation procedure is repeated twice.

E. AuNR Conjugation on PC Biosensor Surface

1-ethyl-3-(3-dimethylaminopropyl) carbodiimide (EDC, Thermo Scientific), and N-hydroxy succinimide (NHS, Thermo Scientific) as SH-PEG-COOH are added to a solution of heterobifunctional polyethylene glycol (SH-PEG-COOH) in water (37.5 µL, 20 µM, Mw=5000 g/mol, Jenkem Technology), followed by shaking for 1 h. The pH of the above reaction mixture is adjusted to 7.4 by adding 10× concentrated phosphate buffered saline buffer solution, followed by the addition of rabbit immunoglobulin G (IgG) (10 µL, 75 µM, Mw=150 kDa, Thermo Scientific). The reaction mixture is incubated for 2 h, and then filtered to remove any byproduct during the reaction using a 50 kDa filter. The final SH-PEG-IgG conjugates solution (0.75 µM) is obtained after washing with phosphate buffered saline buffer twice. AuNR-IgG conjugates solution is prepared by adding 50 µL SH-PEG-IgG conjugates solution to 1 mL twice centrifuged AuNR solution with incubation for 1 h. The amount of SH-PEG-IgG is optimized to obtain maximum coverage of IgG on AuNR surface. Then the PC surface is exposed to AuNR-IgG conjugates solution for 30 mins, followed by rinsing with deionized water to remove the loosely bound nanorods.

IV. RESULTS AND DISCUSSION

A. Electromagnetic Modeling Results

The FDTD computer simulation results exhibit the shift of reflection spectra (Fig. 3a) and the distribution of the electric fields (Fig. 3b) on the PC surface. It also demonstrates an expected establishment of an evanescent electric field at the PC surface with enhanced field magnitude that develops due to the formation of electric field standing waves. With the physical dimensions of the fabricated PC device, FDTD simulation result predicts a resonant reflection wavelength of $\lambda_{PC} \sim 620$ nm and a reflection efficiency $I \sim 96\%$. Fig.3c shows the electric field distribution around an AuNR.

B. AuNR Synthesis and Functionalization

We next studied the AuNR synthesis and functionalization as biosensing tags. Fig. 4 shows a synthesized gold nanorods with size of $\sim 30 \times 30 \times 65$ nm^3 resulting with a desired resonant optical absorption spectra around ~620 nm (which matches the PC resonant wavelength). Then we employed Rabbit IgG as model capture biomolecule and anti-Rabbit IgG as model target bioanalyte to demonstrate the detection of antibody-antigen binding. In this setup, thiol-terminated polyethylene glycol (SH-PEG), a hydrophilic polymer, serves as a flexible linker to increase the accessibility of IgG
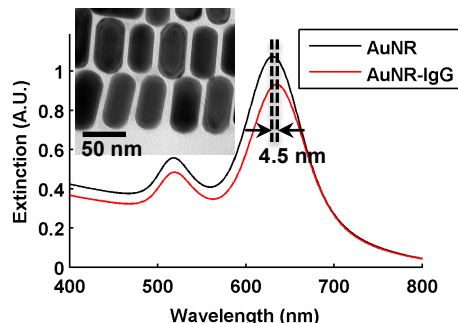

Figure 4. AuNR conjugation with SH-PEG-IgG with UV-vis extinction spectra confirmation. Inset: TEM image of AuNRs.
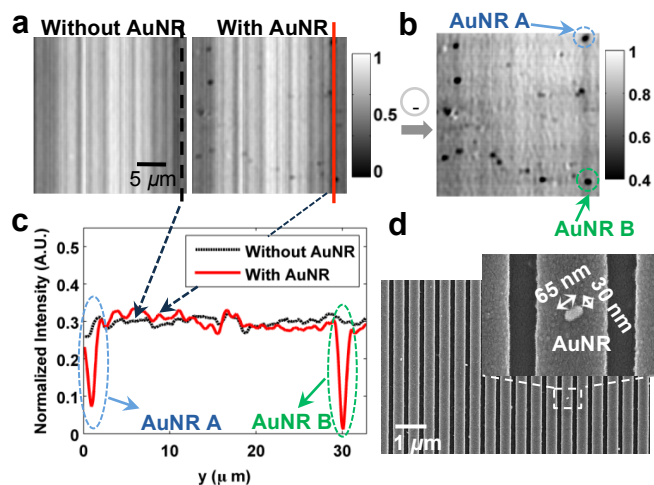
Figure 5. PCEM detection of protein-protein binding. (a) PCEM detected PIV images for the (b) difference between without and with AuNR-IgG on the PC surface. (c) Two representative cross-section lines of the normalized intensity images with/without two AuNRs-IgG. (d) SEM images of AuNR-IgG attached to the PC biosensor surface. Inset: Zoomed in image.

to target bioanalyte [18, 19]. The UV-vis extinction spectra shifts ~4.5 nm after adding SH-PEG-IgG to AuNR solution, which confirms the AuNR conjugation with IgG molecules.

C. NP-PCEM Detection of Antibody-Antigen Binding

Finally, we studied the PC biosensor's ability to detect target bioanalytes binding with immobilized antibody on the PC biosensor surface using NP-PCEM imaging system. Exposing the PC biosensor surface to AuNR-IgG conjugates resulted in specific binding to anti-IgG (SEM images shown in Fig. 5c), which can be detected as a PIV reduction in the area absorbed with AuNR. Fig. 5a shows the mathematical difference between two PIV images taken before and after AuNR-IgG attachment and one representative cross-section lines in the PIV images (Fig. 5b). It demonstrates that NP-PCEM imaging system can successfully detect the intensity reduction in presence of individual AuNR-IgG, which bound to the immobilized Anti-IgG on the PC biosensor surface.

V. CONCLUSION

In conclusion, we report the detection of antibody-antigen binding with single nanoparticle resolution using a novel nanosensing approach of NP-PCEM. We demonstrate that functionalized gold nanorods tags can be detected through their optical absorption due to substantially reducing the resonant reflection efficiency through quenching of the PC resonance. Meanwhile, the photonic crystal resonance can be matched by tuning the LSPR property of the gold nanorods, which substantially increases the sensitivity of this approach. The results reported here lay the foundation for the use of nanoparticles as biosensing tags for biomolecular assays performed upon a PC surface and measured by a NP-PCEM instrument. We envision the development of sandwich-style assays in which the PC surface is prepared with detection molecules for low-concentration analytes (such as cancer biomarkers or viral particles), where nanoparticle tags prepared with capture antibodies can decorate the captured

analyte. Such an approach may enable multiplexed detection of analytes with single-molecule resolution.

REFERENCES

[1] M. R. Lee and P. M. Fauchet, "Nanoscale microcavity sensor for single particle detection," *Opt Lett,* vol. 32, pp. 3284-6, Nov 15 2007.

[2] J. Zhu, S. K. Ozdemir, Y. Xiao, L. Li, L. He, D. Chen, and L. Yang, "On-chip single nanoparticle detection and sizing by mode splitting in an ultrahigh-Q microresonator (vol 4, pg 46, 2010)," *Nature Photonics,* vol. 4, pp. 46-49, Feb 2010.

[3] A. Gupta, D. Akin, and R. Bashir, "Single virus particle mass detection using microresonators with nanoscale thickness," *Applied Physics Letters,* vol. 84, pp. 1976-1978, Mar 15 2004.

[4] R. V. Olkhov, J. D. Fowke, and A. M. Shaw, "Whole serum BSA antibody screening using a label-free biophotonic nanoparticle array," *Anal Biochem,* vol. 385, pp. 234-241, Feb 15 2009.

[5] C. Novo, A. M. Funston, and P. Mulvaney, "Direct observation of chemical reactions on single gold nanocrystals using surface plasmon spectroscopy," *Nature Nanotechnology,* vol. 3, pp. 598-602, Oct 2008.

[6] G. J. Nusz, S. M. Marinakos, A. C. Curry, A. Dahlin, F. Hook, A. Wax, and A. Chilkoti, "Label-free plasmonic detection of biomolecular binding by a single gold nanorod," *Analytical Chemistry,* vol. 80, pp. 984-989, Feb 15 2008.

[7] K. M. Mayer, S. Lee, H. Liao, B. C. Rostro, A. Fuentes, P. T. Scully, C. L. Nehl, and J. H. Hafner, "A label-free immunoassay based upon localized surface plasmon resonance of gold nanorods," *ACS Nano,* vol. 2, pp. 687-692, Apr 2008.

[8] B. T. Cunningham, B. Lin, J. Qiu, P. Li, J. Pepper, and B. Hugh, "A plastic colorimetric resonant optical biosensor for multiparallel detection of label-free biochemical interactions," *Sensor Actuators B-Chem,* vol. 85, pp. 219-226, Jul 25 2002.

[9] B. T. Cunningham, P. Li, B. Lin, and J. Pepper, "Colorimetric resonant reflection as a direct biochemical assay technique," *Sensor Actuators B-Chem,* vol. 81, pp. 316-328, Jan 5 2002.

[10] B. T. Cunningham, P. Li, S. Schulz, B. Lin, C. Baird, J. Gerstenmaier, C. Genick, F. Wang, E. Fine, and L. Laing, "Label-free assays on the BIND system," *J Biomol Screen,* vol. 9, pp. 481-490, Sep 2004.

[11] N. Ganesh, I. D. Block, and B. T. Cunningham, "Near ultraviolet-wavelength photonic-crystal biosensor with enhanced surface-to-bulk sensitivity ratio," *Applied Physics Letters,* vol. 89, pp. 023901-023903, Jul 2006.

[12] J. O. Grepstad, P. Kaspar, O. Solgaard, I. R. Johansen, and A. S. Sudbo, "Photonic-crystal membranes for optical detection of single nano-particles, designed for biosensor application," *Optics Express,* vol. 20, pp. 7954-7965, Mar 26 2012.

[13] R. Vedula, G. Daaboul, A. Reddington, E. Ozkumur, D. A. Bergstein, and M. S. Unlu, "Self-referencing substrates for optical interferometric biosensors," *J Mod Opt,* vol. 57, pp. 1564-1569, Sep 20 2010.

[14] G. G. Daaboul, A. Yurt, X. Zhang, G. M. Hwang, B. B. Goldberg, and M. S. Unlu, "High-throughput detection and sizing of individual low-index nanoparticles and viruses for pathogen identification," *Nano Lett,* vol. 10, pp. 4727-31, Nov 10 2010.

[15] M. R. Monroe, G. G. Daaboul, A. Tuysuzoglu, C. A. Lopez, F. F. Little, and M. S. Unlu, "Single nanoparticle detection for multiplexed protein diagnostics with attomolar sensitivity in serum and unprocessed whole blood," *Analytical Chemistry,* vol. 85, pp. 3698-706, Apr 2 2013.

[16] S. Person, B. Deutsch, A. Mitra, and L. Novotny, "Material-specific detection and classification of single nanoparticles," *Nano Lett,* vol. 11, pp. 257-61, Jan 12 2011.

[17] Y. Zhuo, H. Hu, W. Chen, M. Lu, L. Tian, H. Yu, K. D. Long, E. Chow, W. P. King, S. Singamaneni, and B. T. Cunningham, "Single nanoparticle detection using photonic crystal enhanced microscopy," *Analyst,* vol. 139, pp. 1007-15, Mar 7 2014.

[18] L. Tian, J. J. Morrissey, R. Kattumenu, N. Gandra, E. D. Kharasch, and S. Singamaneni, "Bioplasmonic paper as a platform for detection of kidney cancer biomarkers," *Analytical Chemistry,* vol. 84, pp. 9928-9934, 2012.

[19] L. Tian, E. Chen, N. Gandra, A. Abbas, and S. Singamaneni, "Gold Nanorods as Plasmonic Nanotransducers: Distance-Dependent Refractive Index Sensitivity," *Langmuir,* vol. 28, pp. 17435-17442, Dec 18 2012.